Published in final edited form as:
J Immunol. 2015 March 1; 194(5): 2140–2147. doi:10.4049/jimmunol.1402503.

Interleukin33 Is Required for Disposal of Unnecessary Cells during Ovarian Atresia through Regulation of Autophagy and Macrophage Migration

Jean Wu[*], **Colin Carlock**[*], **Cindy Zhou**[*,3], **Susumu Nakae**[†], **John Hicks**[‡], **Henry P. Adams**[§], and **Yahuan Lou**[*]

[*]Department of Diagnostic Sciences, School of Dentistry, University of Texas Health Science Center at Houston, Houston, TX 77054, USA

[†]Department of Allergy and Immunology, National Research Institute for Child Health and Development, Tokyo 157-8535, Japan

[‡]Department of Pathology, Baylor College of Medicine, Houston, TX 77030, USA

[§]Department of Developmental Biology, University of Texas M.D. Anderson Cancer Center, Houston, TX 77030, USA

Abstract

Physiological processes such as ovarian follicle atresia generate large amounts of unnecessary cells or tissue detritus, which needs to be disposed of rapidly. Interleukin33 (IL33) is a member of the IL1 cytokine gene family. Consecutive expression of IL33 in a wide range of tissues has hinted at its role beyond immune defense. We have previously reported a close correlation between IL33 expression patterns and ovarian atresia. Here, we demonstrated that IL33 is required for disposal of degenerative tissue during ovarian atresia using *Il33*$^{-/-}$ mice. Deletion of the Il33 gene impaired normal disposal of atretic follicles, resulting in massive accumulations of tissue wastes abundant with aging-related catabolic wastes such as lipofuscin. Accumulation of tissue wastes in *Il33*$^{-/-}$ mice, in turn, accelerated ovarian aging and functional decline. Thus, their reproductive lifespan was shortened to 2/3 of that for *Il33*$^{+/-}$ littermates. IL33 orchestrated disposal mechanism through regulation of autophagy in degenerating tissues and macrophage migration into the tissues. Our study provided direct evidence supporting an expanded role of IL33 in tissue integrity and aging through regulating disposal of unnecessary tissues or cells.

Keywords

Cytokine; degeneration; aging; autophagy; reproductive immunology; ovaries

Correspondence: Dr. Yahuan Lou, Department of Diagnostic and Biomedical Sciences, SD, The University of Texas HSC at Houston, 5326 Behavioral and Biomedical Science Building (BBSB), 1941 East Road, Houston, TX 77054, Phone: 713-486-4059, Fax: 713-486-0450, Yahuan.lou@uth.tmc.edu.
[3]**Current address:** Department of Cancer Biology, SD, University of Maryland, 650 W Baltimore St, Baltimore, MD 21201, USA

Introduction

Physiological processes are often accompanied with the generation of tissue detritus or catabolic wastes from unwanted cells or substances. Rapid and proper disposal of these wastes is vital for maintaining tissue integrity and functionality. Accumulation of tissue wastes or catabolic products such as reactive oxidative species and lipofuscin accelerates tissue or cell aging processes (1, 2). Ovaries are active organs. Massive cell death or tissue destruction often follows frequently occurring physiological events. Ovarian atresia, a degenerative process for oocytes, occurs in more than 99% of follicles (3). Speedy removal of those atretic follicles is crucial for keeping oocytes/follicles healthy. Apoptosis in granulosa cells has been considered the underlying mechanism of atresia (4). However, it remains unclear if apoptosis occurs in the majority of follicular cells during atresia. Furthermore, it is unknown how this large quantity of degenerative tissue is rapidly removed or disposed of.

Interleukin33 (IL33) is a new member of the IL1 cytokine gene family (5). As it has a nuclei-binding domain, IL33 is often detected as a nuclear protein (6). IL33 has been implicated in regulation of Th2 type T cell response and innate immunity (5, 7). It also function as an alarmin in defense against viral infection (8). However, mounting evidence suggests its role beyond immune response because of its constitutive expression in many normal tissues (9, 10). We have previously reported IL33 expression in ovaries (11). The IL33-expressing cells are largely endothelial cells surrounding developing follicles or in the inner theca of ovulating follicles. IL33 expression level is closely associated with the estrous cycle and ovulation. Cleaved IL33 is rapidly released prior to the wave of atresia and migration of microphages during estrous cycle. These data suggested its potential roles in these ovarian functions. Using *Il33*$^{-/-}$ mice, we investigate the involvement of IL33 during these physiological degenerative processes.

Materials and Methods

Mice and their treatment

C57BL/6 mice were purchased from Harlan (Indianapolis, IN, USA). *Il33*$^{tm1(KOMP)Vlcg}$ (*Il33*$^{-/-}$) mouse strain was created from ES cell clone 12663E-H2 (Regeneron Pharmaceuticals, Inc.) and made into live mice by the KOMP Repository (WWW.KOMP.org) and the Mouse Biology Program (www.mousebiology.org) at the University of California Davis (12). The strategy for deletion of *Il33* gene is shown in Figure 1A. The mice were maintained in the animal facility at the University of Texas Health Science Center at Houston and allowed to acclimate for a minimum of seven days. All animal procedures in this study were approved by institutional animal welfare committee. Ovaries were harvested and fixed in 2% paraformaldehyde or snap-frozen in liquid nitrogen. In some cases, ovaries were used for isolation of total RNA with a kit from Ambion (Austin TX, US). For induction of superovulation in mice, a previously published method was adapted (13). Briefly, the animals were injected with eCG (equine chorionic gonadotropin)(Sigma, St. Louis, MO) at 5 IU/mouse intraperitoneally (i.p.). After 48 hours, the mice were injected i.p. with hCG (human chorionic gonadotropin), 5 IU/mouse (Sigma, St. Louis, MO).

Genotyping

For genotyping of mice, genomic DNA was isolated from tail-tip of the new born and used for PCR based genotyping. Two pair s of primers for the vector (*Neo*, ^{5}GCAGCCTCTGTTCCACATACACTTCA^{3}, and ^{5}TCTTCACAGAAAGGGCTGATCTGAGG^{3}) and endogenous *Il33* gene (*Reg-Il33*, ^{5}CTATGGCCAAATACCCAGCAGAAGC^{3}, and ^{5}ATGAGAAGTCCCTGGAAGCTAAGGC^{3}) were used for PCR (Fig. 1A). PCR was performed for 40 cycles at 94°C for15 seconds, 65°C for 40 seconds, and 72C for 40 seconds, which resulted in product DNAs with 653bp for *Neo* and 132bp for *Reg-Il33*. Typical results for each genotype, i.e. $Il33^{+/+}$, $Il33^{+/-}$, $Il33^{-/-}$, are shown (Fig. 1B). After the animals were used for experiments, their ovaries or other tissues were further used to confirm their genotypes by detection of IL33 proteins by western blot or immunofluorescence (11).

Histology, electron microscopy and detection of lipofuscin

Ovaries or other tissues were fixed in Bouin's solution for routine H-E staining. Five μm sections were cut through entire ovaries, and three sections with the largest cross sections were used for counting normal or atretic follicles, or corpora lutea. Developing follicles were further classified into type 3 to 8 according to an established method (14). Each type of follicles was separately counted and compared between WT and $Il33^{-/-}$ mice. For transmission electron microscopy (TEM), a small piece of ovaries (0.5 mm^3) was fixed in 4% of paraformaldehyde and further treated by Osmium tetroxide. Ultrathin sections were processed by a routine method for electron microscopic observation. TEM imagines were recorded on film or digitally. Two methods were used for detection of ovarian lipofuscin. The first method was Sudan Black B staining following a published method (15). Briefly, non-fixed frozen ovarian sections were observed by fluorescent microscope through three channels and autofluorescent images were recorded. The sections were then processed for Sudan Black B staining, and observed by the same microscope under bright field. The images from the two were paired and analyzed. The second method was based on lipofuscin's special fluorescent emission peak. Briefly, three UV lasers were used for excitation, and emitting fluorescence spectra (436–714nm with an average interval of 5nm) from autofluorescent materials on ovarian sections were recorded with a confocal microscope from Nikon. Emission peaks for lipofuscin were identified following published papers (16, 17).

Long-term fertility trail

One $Il33^{-/-}$ female and one $Il33^{+/-}$ litter mate were housed with a WT fertile male in a cage. Males were rotated every four days. Sign of mating (presence of vaginal plug) in each female was examined daily. Upon sign of pregnancy, the female was moved to an isolated cage for delivery. Litter size was recorded immediately after delivery. Mothers were allowed to lactate the neonatal for three weeks, and then was retuned the original cage for mating. If a female failed to become pregnant for 7 weeks continuous mating with multiple males, the mouse was considered infertile. The date for its last delivery was used for calculating

reproductive lifespan. If a female was never able to conceive, the date for starting mating was used for calculation.

Abs

Biotin labeled anti-mouse MHC class II molecules IA/IE (rat IgG2a, 2G9) mAb was purchased from BD Biosciences (San Jose, CA, USA). Biotinylated goat anti-mouse IL33 Ab and rat anti-mouse IL33 mAb (clone 396118) were obtained from R&D System (Minneapolis, MN, USA) or ProSci (Charleston, SC, USA). FITC-labeled or non-labeled anti-β-actin Abs and purified anti-ZP3 (IE-10) mAbs were from Sigma-Aldrich (St. Louis, MO, USA). Secondary reagents Alexa-555, Alexa-594 and Alexa-647-labeled (Life Technologies, Carlsbad, CA, USA) and PE labeled (BD Biosciences) streptavidin were used to visualize biotin labeled antibodies. Biotin/avidin and anti-mouse CD16/32 mAb (D34–485, BD Biosciences) was used for blocking non-specific IgG binding. Various immunoglobulin isotypes used as negative controls were from BD Biosciences.

Immunofluorescence, TUNEL staining, and quantitation of cells on sections

Ovaries, fixed or non-fixed depending on activity of the Abs to be used, were frozen and 3 μm frozen sections were cut. All sections were blocked in 3% BSA with CD16/32 antibodies. If biotin labeled antibodies were to be used, a biotin and avidin blocking step was added (Vector BioLab, Philadelphia, PA, USA). The ovarian sections observed by a fluorescent microscope (Nikon 80i Eclipse, Tokyo, Japan) and digital images were captured and analyzed with NIS Elements 3.2 from Nikon. In some cases, fluorescent images were taken by a confocal microscope in M.D. Anderson Cancer Center (Houston, TX, USA). For TUNEL staining, a kit (In Situ Cell Death Detection Kit, Fluorescein, Roche, Nutley, NJ, USA) was used following manufacturer's instruction. For quantitation of macrophages, 6 mice were randomly selected from each group, and 3 frozen sections were randomly cut from each ovary. The ovarian sections were stained by Ab to each macrophage marker together with other antibodies. Immunofluorescent images were taken. All atretic developing follicles were identified. The atretic stage of each atretic follicle was determined based on presence of apoptotic cells for early stage, and collapsing zona pellucida/deformation for mid stage. $CD68^+$ and IA^+ macrophages were manually counted for each follicle respectively. The results were expressed as macrophages/atretic follicle section.

Western blot

Ovaries were harvested and immediately homogenized on ice in an extraction buffer containing a protease inhibitor cocktail (Sigma-Aldrich, St Louis, MO, USA). After centrifugation at 10,000*g* for 15 min at 4°C, the supernatant was carefully removed and its protein concentration measured. The ovarian extracts were mixed 1:1 with SDS sample buffer. Ten μg of protein was loaded on a 12.5% SDS-PAGE and ran at a constant current. After transfer, a membrane (Immobilon-P PVDF, Millipore, Billerica, MA, USA) was used for detection of target proteins. For detection of LC3, the membrane was simultaneously incubated with biotin-labeled anti-LC3 Ab (rabbit, Novus, Littleton, CO, USA) and anti-β-actin mAb (AC-15, Sigma). The membrane was further incubated with IRDye®800CW labeled anti-rabbit IgG and IRDye® 680LT anti-mouse IgG Abs (LI-COR, Lincoln, NE).

The membrane was scanned on an infrared fluorescence scanner (Odyssey, LI-COR). A similar method was used for detection of IL33 proteins.

Statistics

T-tests were used for comparison between 2 groups. Statistical significances were indicated by *($p<0.05$), **($p<0.01$), or ***($p<0.001$). Before pooling data from multiple groups, data from each experiment was statistically compared to rule out any differences among them. Linear regression test was used for analysis of correlation between ages and ovarian autofluorescence in WT and *Il33*$^{-/-}$ females, respectively; r^2 and *P* value for deviation from zero was calculated for each progression. Finally, slopes of the two linear progressions were compared for statistical significance.

Results

Deletion of the Il33 gene leads to massive accumulation of abnormally degrading atretic follicles in mouse ovaries

We have reported that a unique spatial and temporal expression pattern of IL33 in ovaries is closely associated with ovarian atresia surge and ovulation. The sudden release of IL33 from nuclei prior atresia surge and ovulation suggests a potential role of IL33 in these ovarian events (11). To further determine IL33's roles, an *Il33*$^{-/-}$ mutant was generated through deletion of *Il33* gene in a C57BL/6 (B6) mouse (Fig. 1A and B). Characterization of *Il33*$^{-/-}$ mice demonstrated a complete lack of IL33 in their ovaries at the protein level by either western blot or immunofluorescence (Fig. 1C and D). No abnormalities were found in the organs of *Il33*$^{-/-}$ mice at up to ages of 20 wks. Similar to their WT or *Il33*$^{+/-}$ litter mates, female *Il33*$^{-/-}$ mice matured at 6–8 weeks and were initially fertile. However, the presence of large quantities of autofluorescent material in young *Il33*$^{-/-}$ ovaries was observed (Fig. 2A). The autofluorescence appeared as early as 3–5 weeks (puberty), rapidly increased after 5–7 weeks (sexually mature), and became massive at 15–20 weeks (reproductive peak), which greatly expanded the interstitial tissue (Fig. 2A and B). In contrast, WT mice had only a few autofluorescent granules during their reproductive peak (Fig. 2A). The amount of autofluorescence also increased with age in WT mice (Fig. 2B). However, it never reached the level seen in young *Il33*$^{-/-}$ mice even after 50 weeks (Fig. 2B). Linear progression between ovarian autofluorescence and age was analyzed for *Il33*$^{-/-}$ and WT mice, respectively (Fig. 2B). Statistical comparison between slopes of the two linear progresses showed that *Il33*$^{-/-}$ ovaries showed a 3.2-fold faster accumulation of autofluorescence than WT ovaries ($p<0.0001$)(Fig. 2B). The autofluorescence in *Il33*$^{-/-}$ ovaries was emitted from numerous spherical bodies with diameters of 20–60 μm (Fig. 2C). Ultrastructurally, each spherical body was surrounded by cells resembling theca, and contained dislocated degrading organelles, myelin figures (undigested plasma membranes) and granulosa cell nuclei (Fig. 2D). Thus, these autofluorescence-emitting structures were abnormally collapsing atretic follicles. Sudan Black B staining and fluorescent spectra analysis further showed that they were abundant with autofluorescent age pigment lipofuscin (Fig. 2E and F). Therefore, deletion of *Il33* gene impaired normal disposal of atretic follicles, resulting in accumulation of large amounts of catabolic waste.

Accelerated ovarian function decline and shortened reproductive life in Il33$^{-/-}$ female mice

Catabolic wastes such as lipofuscin have been implicated in tissue aging and degeneration in organs such as eyes and the central nervous system (18–21). We examined if the accumulation of wastes from abnormally degrading atretic follicles in *Il33*$^{-/-}$ mice affected their ovarian functions. *Il33*$^{-/-}$ mice at their reproductive peak showed significantly fewer total developing follicles and corpora lutea compared to age-matched WT mice (Fig. 3A). The reduction in developing follicles was especially significant for type 3, 4 and 7 follicles (Fig. 3B). Upon eCG/hCG-induced superovulation, the number of eggs ovulated by *Il33*$^{-/-}$ mice was reduced to 65% of age-matched WT mice, suggesting a significantly shrunken oocyte reservoir (Fig. 3C). A long-term fertility trial under natural mating was performed to assess ovarian aging. The average reproductive lifespan, as indicated by the age for the last successful delivery, in *Il33*$^{-/-}$ females was shortened to 2/3 of that for *Il33*$^{+/-}$ littermates (Fig. 3D). *Il33*$^{-/-}$ females delivered fewer litters than their *Il33*$^{-/+}$ littermates (3.15±0.61 vs 5.90±0.48) during their whole reproductive life (Fig. 3E). Thus, accumulation of tissue waste from the impaired disposal of atretic follicles had accelerated ovarian aging, resulting in much earlier cessation of ovarian function.

Failed disposal of atretic follicles is associated with impaired migration of macrophages into atretic follicles

We next investigated why deletion of the *Il33* gene impaired disposal of atretic follicles. First, deletion of the *Il33* gene did not affect apoptosis during atresia (Fig. 4A and C). As we have also previously reported, apoptosis occurs transiently at early atresia and only in a small portion of granulosa cells (11). Based on the above results, we concluded that apoptosis is not fully responsible for disposal of atretic follicles. Second, we have reported migration of two subsets of ovarian macrophages into atretic follicles during atresia (11, 22). The first one expresses MHC class II molecule (IA$^+$ macrophages), which invades early atretic follicles with apoptotic cells (Fig. 4A, B). The second one, CD68$^+$ macrophages, invade atretic follicles after mid atresia post wave of apoptosis; they further move to surround oocytes (Fig. 4C). However, invasion of both IA$^+$ and CD68$^+$ macrophages was not observed in *Il33*$^{-/-}$ mice (Fig. 4A–D). Instead, autofluorescent materials emerged in follicular cells after mid atresia; the autofluorescence first appeared in the cells surrounding oocytes (Fig. 4C). Therefore, development of autofluorescence in atretic follicles in *Il33*$^{-/-}$ mice was coincident with failed migration of CD68$^+$ macrophages into the same location.

Failed disposal of atretic follicles is associated with diminished autophagy in follicular cells in Il33$^{-/-}$ mice

It is possible that the autofluorescent materials in *Il33*$^{-/-}$ mice might be remnants of un-phagocytized follicular cells due to failed CD68$^+$ macrophage migration. However, it was questionable if this small number of invading CD68$^+$ macrophages would be able to quickly “cleanup” the massive follicular cells. Autophagy is a mechanism that would allow the rapid disposal of unwanted cells (23). Several previous studies have also suggested a potential role of autophagy in ovarian atresia (24, 25). We first determined whether autophagy was involved in normal atresia in WT mice. Three lines of evidence demonstrated that autophagy was a major mechanism for disposal of granulosa cells in atretic follicles. *First*, LC3

(microtubule-associated protein 1 light chain 3, *atg8*), a critical molecule in autophagy, must transform from LC3-I to LC3-II to form autophagosomes (26, 27). Western blot of ovarian proteins demonstrated the presence of LC3-II (Fig. 5A). *Second*, once formed, autophagosomes with LC3 can be detected as sub-cellular $LC3^+$ granules (28). $LC3^+$ granules were detected in the cytoplasm of granulosa cells only after mid atresia (Fig. 5B). This result also showed a co-occurrence of autophagosome formation and invasion of $CD68^+$ macrophages at mid stage of atresia (Figs. 4C, and 5B). *Third*, electron-microscopy revealed numerous autophagous vacuoles in the granulosa cells of atretic follicles (Fig. 5C, and D). Autophagosomes characterized by double membranes with organelles inside were also observable (inset in Fig. 5D). However, the occurrence of autophagy was not observed in any stages of atretic follicles of $Il33^{-/-}$ mice. *First*, ovarian LC3-II was greatly reduced in $Il33^{-/-}$ mice despite of comparable amount of LC3-I to WT mice (Fig. 5A). *Second*, $LC3^+$ subcellular autophagosomes were not observed in any atretic follicles in $Il33^{-/-}$ mice (Fig. 5B). Failed autophagy in $Il33^{-/-}$ mice was coincident with appearance of autofluorescence. Appearance of autofluorescent lipofuscins, in fact, is a biomarker for declining autophagy (27). Without autophagy and $CD68^+$ macrophages, atretic follicles in $Il33^{-/-}$ simply collapsed. Ultrastructurally, those follicles contained relatively normal but dislocated granulosa cell nuclei and numerous fragmented cytoplasm membranes tangled with degrading organelles. There were no intact plasma membranes and cell boundaries within those collapsing follicles (Fig. 5D). Importantly, autophagous vacuoles were absent in these collapsing follicles (Fig. 5D). We conclude that *Il33* gene deletion had impaired autophagy in atretic follicles.

Discussion

Using $Il33^{-/-}$ mice, we demonstrated that deletion of the *Il33* gene impaired the mechanism for disposal of unnecessary tissues, i.e. atretic follicles, despite normal apoptosis in follicular cells. As a result, catabolic wastes from abnormally collapsing follicles, such as lipofuscins, accumulated, which in turn significantly affected ovarian functions and reproductive life of the host. Regulation of disposal mechanisms for unnecessary cells or tissue catabolic wastes is critical for keeping tissues' integrity and functionality, especially over a relatively long-term. Accumulation of tissue wastes has been considered one of the major factors for exacerbating tissue/cell aging processes (1, 2). Therefore, IL33 may play a critical role in controlling tissue aging by regulating the disposal of unwanted cells or tissue wastes in the ovaries, although it does not directly participate in any ovarian functions. Potential functions of IL33 have been explored intensively in the past several years. Those functions include regulation or promotion of Th2 type T cell response, allergic response, and innate immunity (5, 7). IL33 also acts as an alarmin to enhance $CD8^+$ T cell response during viral infection (8). In contrast to those previous findings, our discovery reveals a unique function of IL33 in controlling the aging process rather than in immune defense.

The observations from this study, as well as our previous ones, revealed certain sequential events during ovarian atresia: 1) a short transient period for apoptosis in a small number of follicular cells at early atresia, 2) invasion of MHC class II IA^+ macrophages into early atretic follicles, and 3) autophagy in follicular cells, which co-occurred with 4) invasion of $CD68^+$ macrophages at mid atresia post transient wave of apoptosis. Deletion of the *Il33*

gene impaired all events but apoptosis. Impairments in autophagy and $CD68^+$ macrophage migration were coincident with development of autofluorescent materials and abnormal collapse of follicles in *Il33*$^{-/-}$ mice, suggesting their direct involvement in disposal of atretic follicles. Thus, the above results allow us to hypothesize disposal mechanism for atretic follicles post apoptosis as following: under regulation of IL33, the majority of follicular cells are first self-digested through autophagy, and the minimal remaining catabolic wastes and tissue debris are then phagocytized by invading $CD68^+$ macrophages. Apoptosis is an early event during atresia for the death in a limited number of granulosa cells but not a disposal mechanism for atretic follicles. In addition, the majority follicular cells do not undergo apoptosis. It is most likely that autophagy is a major pathway for the death of follicular cells.

What is the role of those IA^+ macrophages which invade atretic follicles at the early stage, as their invasion is also regulated by IL33? Unlike $CD68^+$ macrophages, invading IA^+ macrophages showed much less phagocytic activity (22). The following reasons suggest that IA^+ macrophages but not IL33 may induce autophagy in follicular cells during atresia. *First*, temporally, cleaved IL33 is released prior to atresia wave (11). However, autophagy occurs at mid atresia and post IA^+ macrophages' invasion (Fig. 4). Cleaved IL33 also has a very short half-life (28). The time gap between its release (i.e. prior to atresia) and initiation of autophagy (i.e. mid stage) may not guarantee continued activity of IL33. *Second*, spatially, IL33 is expressed in the endothelia of veins surrounding follicles (11). It would be almost impossible for IL33 to pass the multiple tissue barriers to reach all follicular cells. Finally, previous studies have shown that autophagy can be induced by macrophage-associated molecules (29). Nevertheless, this hypothesis needs to be proved in the near future. It can be tested by examination of autophagy in macrophage-depleted ovaries. In addition, IL33 or anti-IL33 ab may be specifically delivered to ovaries using liposome busting technique, which allows us to observe if the treatment alters IA^+ macrophage migration or autophagy in ovaries of WT or *Il33*$^{-/-}$ mice. Furthermore, we will determine if autophagy is critical for the disposal of atretic follicles through induction or inhibition of autophagy in granulosa cells with special reagents such as rapamycin (30).

Another potential function of invading IA^+ macrophages may be prevention of autoimmunity during tissue death and disposal. During disposal of unwanted follicles, leakage of a large quantity of autoantigens is almost guaranteed. Thus, a tolerance mechanism must exist to prevent or inhibit activation of autoreactive T or B cells. Since atresia is an often occurring physiological process and an unusually large amount of autoantigens are released, this tolerance mechanism is most likely very unique and different from those related to stress response systems and disease tolerance during infection, or pathological tissue damage. These follicle-invading IA^+ macrophages express a high level of MHC class II, and thus, are expected to be excellent antigen presenting cells. They will surely pick up leaking autoantigens from atretic follicles and present them on MHC class II molecules. It is conceivable, however, that the presentation of those autoantigens must not lead to the activation of autoreactive T cells or B cells. Tolerogenic macrophages or dendritic cells have been well described (31, 32). Thus, it is highly possible that these IA^+ macrophages function as one type of tolerogenic antigen presenting cells. They may bring

the leaked antigen from atretic follicles and migrate to regional lymph nodes, where they further selectively inactivate or eliminate the autoreactive T or B cells, which recognize the presented autoantigens. Thus, no autoimmunity against ovarian antigens will be provoked during atresia.

It is a common question for all conventional gene knockout animal models that altered phenotypes may be a result of systemic effect of defected genes. However, several results suggest that failed disposal of atretic follicles in our *Il33*$^{-/-}$ mice is not caused by the systemic effect of IL33 deficiency for the following reasons. First, atresia is normally initiated in *Il33*$^{-/-}$ mice as evidenced by presence of apoptotic follicular cells either in timing and quantity. Importantly, deletion of the *Il33* gene did not affect either the estrous cycle or atresia. Second, other ovarian functions such as follicular development, ovulation and maintenance of pregnancy and lactation were largely normal in *Il33*$^{-/-}$ mice with exception of accelerated ovarian aging. Thus, IL33 is not directly involved in those ovarian functions. Third, the endocrine axis is critical for regulation of ovarian functions. We have carefully compared histology of the hypothalamus region of brain and pituitaries of *Il33*$^{-/-}$ mice immediately after their reproductive life (approximately 1.1 years) with those of age-matched *Il33*$^{-/-}$ litter mates. However, no morphological abnormalities were found in *Il33*$^{-/-}$ mice. Although it is unlikely that accelerated aging in *Il33*$^{-/-}$ mice was caused by disturbed endocrine axis, it is necessary to further conduct functional studies to verify our hypothesis in the future. These experiments will include comparisons of pituitary-related hormone level time course or comparison of different groups of pituitary cells through differential staining between WT and *Il33*$^{-/-}$ mice. Nevertheless, ultimate evidence for IL33's direct role in disposal of atretic follicles should be from an animal model with disturbed IL33 expression or defected autophagy only in ovaries. Alternatively, we may conditionally knockout *Il33* gene or autophagy related gene in granulosa cells. This is one of our goals in the near future. Finally, it will be important to explore IL33 receptors in ovaries, which is critical for understanding the IL33 regulated disposal mechanisms. ST2 has been identified as the IL33 receptor (7, 8). We have previously reported elevated ST2 mRNA level, together with transitional expression of IL33 during ovulation (11). Our preliminary study showed that ST2 was not expressed by IA^{+} or CD68^{+} macrophages. We are currently investigating which ovarian cells express ST2, because this will be the first critical step to understand IL33 mediated signal pathways.

An IL33-regulated autophagy-macrophage mechanism is required for disposal of degenerative tissues in ovaries in order to maintain ovarian tissue integrity and to decelerate its aging process. The significances of our finding should be highlighted. *First*, our discovery contributes to a fuller understanding of ovarian atresia. *Second*, the disposal mechanism described in this paper may be used to explain several idiopathic human ovarian disorders such as premature ovarian failure and premature ovarian aging. These disorders are common causes of female infertility, and characterized by accelerated tissue aging and cessation of ovarian function at a young age with unknown etiology in more than 65% of cases (33). It will be interesting to see if these idiopathic cases are related to deficiencies in disposal mechanisms. *Third*, our discovery raises a possibility of a similar mechanism in other tissues. Several previous studies have hinted at this possibility. IL33 is widely

expressed in normal tissues including nerve system and cardiovascular system (9, 10, 34, 35). A human genetic study has already linked *Il33* gene to neurodegenerative diseases in aged people (36). In addition, impaired autophagy has been implicated in several human age-related degenerative diseases (37, 38). It will be interesting to ask if IL33 is also the upstream regulator of autophagy in those organs.

Acknowledgments

We thank Dr. O. Chunakava for analysis of autofluorescent spectrum, Ms K. Tatum for technical help, and institutional histology core facility for ovarian histology. Electron microscopy was conducted in Texas Children's Hospital.

Grant Support: This study was supported by NIH R01 HD049613 (Y.L.) and R01 DK077857 (Y. L.). *Il33*$^{-/-}$ colony was maintained through institutional bridging funding.

Abbreviations used in this paper

eCG	equine chorionic gonadotropin
hCG	human chorionic gonadotropin
IL33	Interleukin33
SM-α-actin	smooth muscle α-actin
LC3	microtubule-associated protein 1 light chain 3
TEM	transmission electron microscopy

References

1. Kregel KC, Zhang HJ. An integrated view of oxidative stress in aging: basic mechanisms, functional effects, and pathological considerations. Am. J. Physiol. 2007; 292(1):R18–R36.
2. Jung T, Bader N, Grune T. Lipofuscin: formation, distribution, and metabolic consequences. Ann. NY Acad. Sci. 2007; 1119(1):97–111. [PubMed: 18056959]
3. Faddy MJ. Follicle dynamics during ovarian ageing. Mol. Cell. Endocrinol. 2000; 163(1–2):43–48. [PubMed: 10963872]
4. Hsueh AJW, Billig H, Tsafriri A. Ovarian follicle atresia: a hormonally controlled apoptotic process. Endocrine Rev. 1994; 15(6):707–724. [PubMed: 7705278]
5. Schmitz J, Owyang A, Oldham E, Song Y, Murphy E, McClanahan TK, Zurawski G, Moshrefi M, Qin J, Li X, Gorman DM, Bazan JF, Kastelein RA. IL-33, an interleukin-1-like cytokine that signals via the IL-1 receptor-related protein ST2 and induces T helper type 2-associated cytokines. Immunity. 2005; 23(5):479–490. [PubMed: 16286016]
6. Baekkevold ES, Roussigné M, Yamanaka T, Johansen FE, Jahnsen FL, Amalric F, Brandtzaeg P, Erard M, Haraldsen G, Girard JP. Molecular characterization of NF-HEV, a nuclear factor preferentially expressed in human high endothelial venules. Am. J. Pathol. 2003; 163(1):69–79. [PubMed: 12819012]
7. Oboki K, Ohno T, Kajiwara N, Arae K, Morita H, Ishii A, Nambu A, Abe T, Kiyonari H, Matsumoto K, Sudo K, Okumura K, Saito H, Nakae S. IL33 is a crucial amplifier of innate rather than acquired immunity. Proc. Natl. Acad. Sci. USA. 2010; 107(43):1858–1856.
8. Bonilla WV, Fröhlich A, Senn K, Kallert S, Fernandez M, Johnson S, Kreutzfeldt M, Hegazy AN, Schrick C, Fallon PG, Klemenz R, Nakae S, Adler H, Merkler D, Löhning M, Pinschewer DD. The Alarmin interleukin-33 drives protective antiviral CD8^{+} T cell responses. Science. 2012; 335(6071): 984–989. [PubMed: 22323740]

9. Yasuoka S, Kawanokuchi J, Parajuli B, Jin S, Doi Y, Noda M, Sonobe Y, Takeuchi H, Mizuno T, Suzumura A. Production and functions of IL-33 in the central nervous system. Brain Res. 2011; 1385:8–17. [PubMed: 21349253]
10. Pichery M, Mirey E, Mercier P, Lefrancais E, Dujardin A, Ortega N, Girard JP. Endogenous IL-33 is highly expressed in mouse epithelial barrier tissues, lymphoid organs, brain, embryos, and inflamed tissues: in situ analysis using a novel Il-33–LacZ gene trap reporter strain. J. Immunol. 2012; 188(7):3488–3495. [PubMed: 22371395]
11. Carlock C, Wu J, Zhou C, Tatum K, Adams HP, Tan F, Lou Y. Unique temporal and spatial expression patterns of IL-33 in ovaries during ovulation and estrous cycle are associated with ovarian tissue homeostasis. J. Immunol. 2014; 193(1):161–169. [PubMed: 24860190]
12. Valenzuela DM, Murphy AJ, Frendewey D, Gale NW, Economides AN, Auerbach W, Poueymirou WT, Adams NC, Rojas J, Yasenchak J, Chernomorsky R, Boucher M, Elsasser AL, Esau L, Zheng J, Griffiths JA, Wang X, Su H, Xue Y, Dominguez MG, Noguera I, Torres R, Macdonald LE, Stewart AF, DeChiara TM, Yancopoulos GD. High-throughput engineering of the mouse genome coupled with high-resolution expression analysis. Nat. Biotechnol. 2003; 21(6):652–659. [PubMed: 12730667]
13. Zhou C, Wu J, Borillo J, Torres L, McMahon J, Lou YH. Potential roles of a special CD8α α^+ cell population and CC chemokine thymus expressed chemokine in ovulation related inflammation. J. Immunol. 2009; 182(1):596–603. [PubMed: 19109193]
14. Pedersen T, Peters H. Proposal for a classification of oocytes and follicles in the mouse ovary. J. Reprod. Fert. 1968; 17:555–557.
15. Georgakopoulou EA, Tsimaratou K, Evangelou K, Fernandez Marcos PJ, Zoumpourlis V, Trougakos IP, Kletsas D, Bartek J, Serrano M, Gorgoulis VG. Specific lipofuscin staining as a novel biomarker to detect replicative and stress-induced senescence-a method applicable in cryo-preserved and archival tissues. Aging. 2013; 5(1):37–50. [PubMed: 23449538]
16. Marmorstein AD, Marmorstein LY, Sakaguchi H, Hollyfield JG. Spectral profiling of autofluorescence associated with lipofuscin, bruch's membrane, and sub-ref deposits in normal and AMD eyes. Invest. Ophthalmol. Vis. Sci. 2002; 43(7):2435–2441. [PubMed: 12091448]
17. Mochizuki Y, Park MK, Mori T, Kawashima S. The difference in autofluorescence features of lipofuscin between brain and adrenal. Zool. Sci. 1995; 12(3):283–288. [PubMed: 7580812]
18. Stojanovic A, Roher AE, Ball MJ. Quantitative analysis of lipofuscin and neurofibrillary tangles in the hippocampal neurons of Alzheimer disease brains. Dementia. 1994; 5(5):229–233. [PubMed: 7951677]
19. Katz ML. Potential role of retinal pigment epithelial lipofuscin accumulation in age-related macular degeneration. Arch. Gerontol. Geriatr. 2002; 34(3):359–370. [PubMed: 14764336]
20. Keller JN, Dimayuga E, Chen Q, Thorpe J, Gee J, Ding Q. Autophagy, proteasomes, lipofuscin, and oxidative stress in the aging brain. Int. J. Biochem. Cell Biol. 2004; 36(12):2376–2391. [PubMed: 15325579]
21. Gray DA, Woulfe J. Lipofuscin and aging: a matter of toxic waste. Sci. Aging Knowl. Environ. 2005; 2005(5):re1.
22. Carlock C, Wu J, Zhou C, Ross A, Adams H, Lou Y. Ovarian phagocyte subsets and their distinct tissue distribution patterns. Reproduction. 2013; 146(5):491–500. [PubMed: 23996136]
23. Rabinowitz JD, White E. Autophagy and metabolism. Science. 2010; 330(6009):1344–1348. [PubMed: 21127245]
24. Choi JY, Jo MW, Lee EY, Yoon BK, Choi DS. The role of autophagy in follicular development and atresia in rat granulosa cells. Fertil. Steril. 2010; 93(8):2532–2537. [PubMed: 20149359]
25. Sánchez E, Martínez E, Vázquez-Nin GH. Immunohistochemical and ultrastructural visualization of different routes of oocyte elimination in adult rats. Eur. J. Histochem. 2012; 56:e17. [PubMed: 22688298]
26. Ichimura Y, Kirisako T, Takao T, Satomi Y, Shimonishi Y, Ishihara N, Mizushima N, Tanida I, Kominami E, Ohsumi M, Noda T, Ohsumi Y. A ubiquitin-like system mediates protein lipidation. Nature. 2000; 408(6811):488–492. [PubMed: 11100732]

27. Stroikin Y, Dalen H, Lööf S, Terman A. Inhibition of autophagy with 3- methyladenine results in impaired turnover of lysosomes and accumulation of lipofuscin-like material. Eur. J. Cell Biol. 2004; 83(10):583–590. [PubMed: 15679103]
28. Luthi AU, Cullen SP, McNeela EA, Duriez PJ, Afonina IS, Sheridan C, Brumatti G, Taylor RC, Kersse K, Vandenabeele P, Lavelle EC, Martin SJ. Suppression of interleukin-33 bioactivity through proteolysis by apoptotic caspases. Immunity. 2009; 31(1):84–98. [PubMed: 19559631]
29. Harris J. Autophagy and cytokines. Cytokine. 2011; 56(2):140–144. [PubMed: 21889357]
30. Sarkar S, Ravikumar B, Floto RA, Rubinsztein DC. Rapamycin and mTOR-independent autophagy inducers ameliorate toxicity of polyglutamine-expanded huntingtin and related proteinopathies. Cell Death Differ. 2009; 16:46–56. [PubMed: 18636076]
31. Manicassamy S, Pulendran B. Dendritic cell control of tolerogenic responses. Immunol. Rev. 2011; 241(1):206–227. [PubMed: 21488899]
32. Wu J, Zhou C, Robertson J, Weng CC, Meistrich ML, Tailor RC, Lou YH. Identification of a bone marrow derived CD8αα^{+} dendritic cell like population in inflamed autoimmune target tissue with capability of inducing T cell apoptosis. J. Leukoc. Biol. 2010; 88(5):831–835. [PubMed: 21041514]
33. Shelling AN. Premature ovarian failure. Reproduction. 2010; 140(5):633–641. [PubMed: 20716613]
34. Miller AM, Xu D, Asquith DL, Denby L, Li Y, Sattar N, Baker AH, McInnes IB, Liew FY. IL-33 reduces the development of atherosclerosis. J. Exp. Med. 2008; 205(2):339–346. [PubMed: 18268038]
35. Hudson CA, Christophi GP, Gruber RC, Wilmore JR, Lawrence DA, Massa PT. Induction of IL-33 expression and activity in central nervous system glia. J. Leuk. Biol. 2008; 84(3):631–643.
36. Chapuis J, Hot D, Hansmannel F, Kerdraon O, Ferreira S, Hubans C, Maurage CA, Huot L, Bensemain F, Laumet G, Ayral AM, Fievet N, Hauw JJ, DeKosky ST, Lemoine Y, Iwatsubo T, Wavrant-Devrièze F, Dartigues JF, Tzourio C, Buée L, Pasquier F, Berr C, Mann D, Lendon C, Alpérovitch A, Kamboh MI, Amouyel P, Lambert JC. Transcriptomic and genetic studies identify IL-33 as a candidate gene for Alzheimer's disease. Mol. Psychiatry. 2009; 14(11):1004–1016. [PubMed: 19204726]
37. Bhuiyan SM, Pattison JS, Osinska H, James J, Gulick J, McLendon PM, Hill JA, Sadoshima J, Robbins J. Enhanced autophagy ameliorates cardiac proteinopathy. J. Clin. Invest. 2013; 123(12): 5284–5297. [PubMed: 24177425]
38. Nixon RA. The role of autophagy in neurodegenerative disease. Nat. Med. 2013; 19(8):983–997. [PubMed: 23921753]

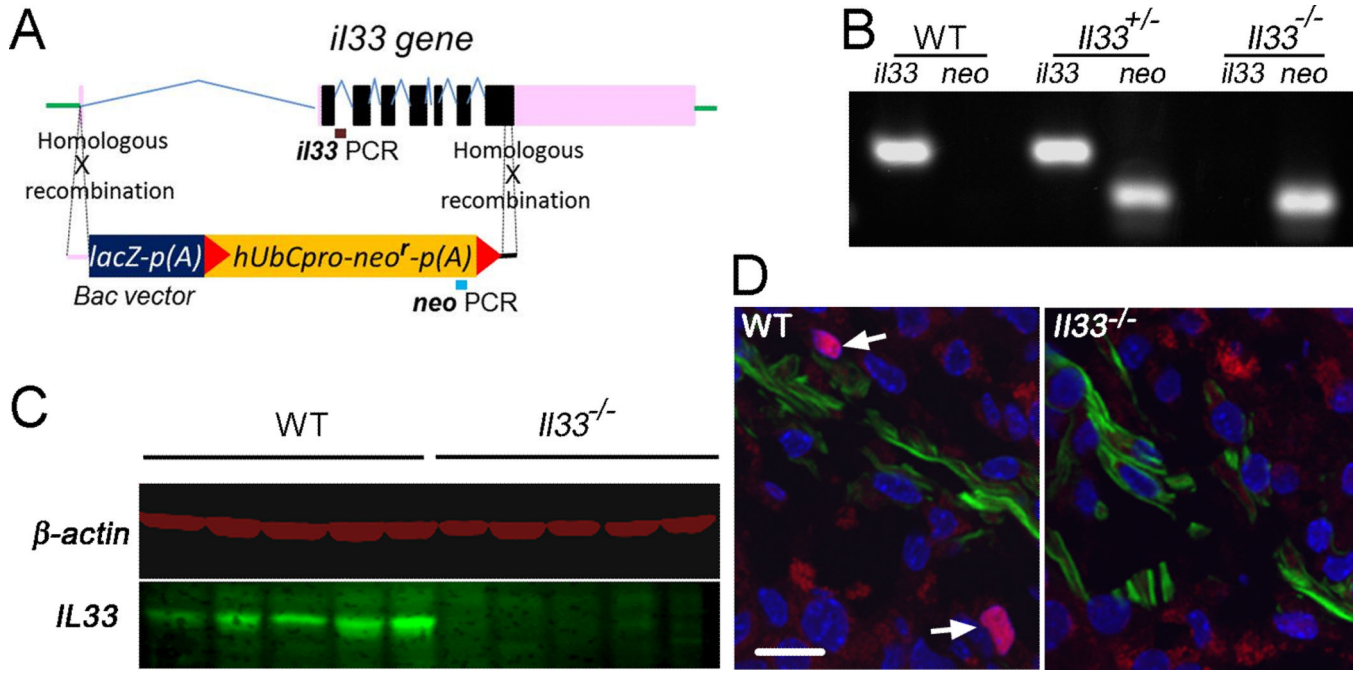

FIGURE 1.

Construction and characterization of *Il33*$^{-/-}$ mouse strain. (**A**) Schematic diagram for knock-out of Il33 genes in genome to create *Il33*$^{-/-}$ mice utilizing homologous recombination via flanking regions through KOMP in C57BL/c (B6) background. The entire Il33 gene is replaced by the vector. (**B**) PCR genotyping for identification of *Il33*$^{-/-}$ mice using two pairs of primers for *neo* in vector and endogenous *Il33* gene, respectively, as shown in A. (**C**) Western blot detection of IL33 protein in the ovaries of WT and *Il33*$^{-/-}$ mice. Results for five representative animals from each group are shown. β–actin is detected in the same blot and used as a protein quantity control. (**D**) Immunofluorescent identification of IL33-expressing cells in the thecal cells of mature follicles undergoing ovulatory process after hCG injection. IL33 is detected as a nuclear protein (red). The sections were counter-stained by α–smooth muscle actin (SM α-actin) antibody (green) to reveal theca layer, and DAPI for nuclei. Arrows indicate nuclear IL33 staining. Nuclear IL33^{+} cells are absent in *Il33*$^{-/-}$ mice. Bar represents 20 μm.

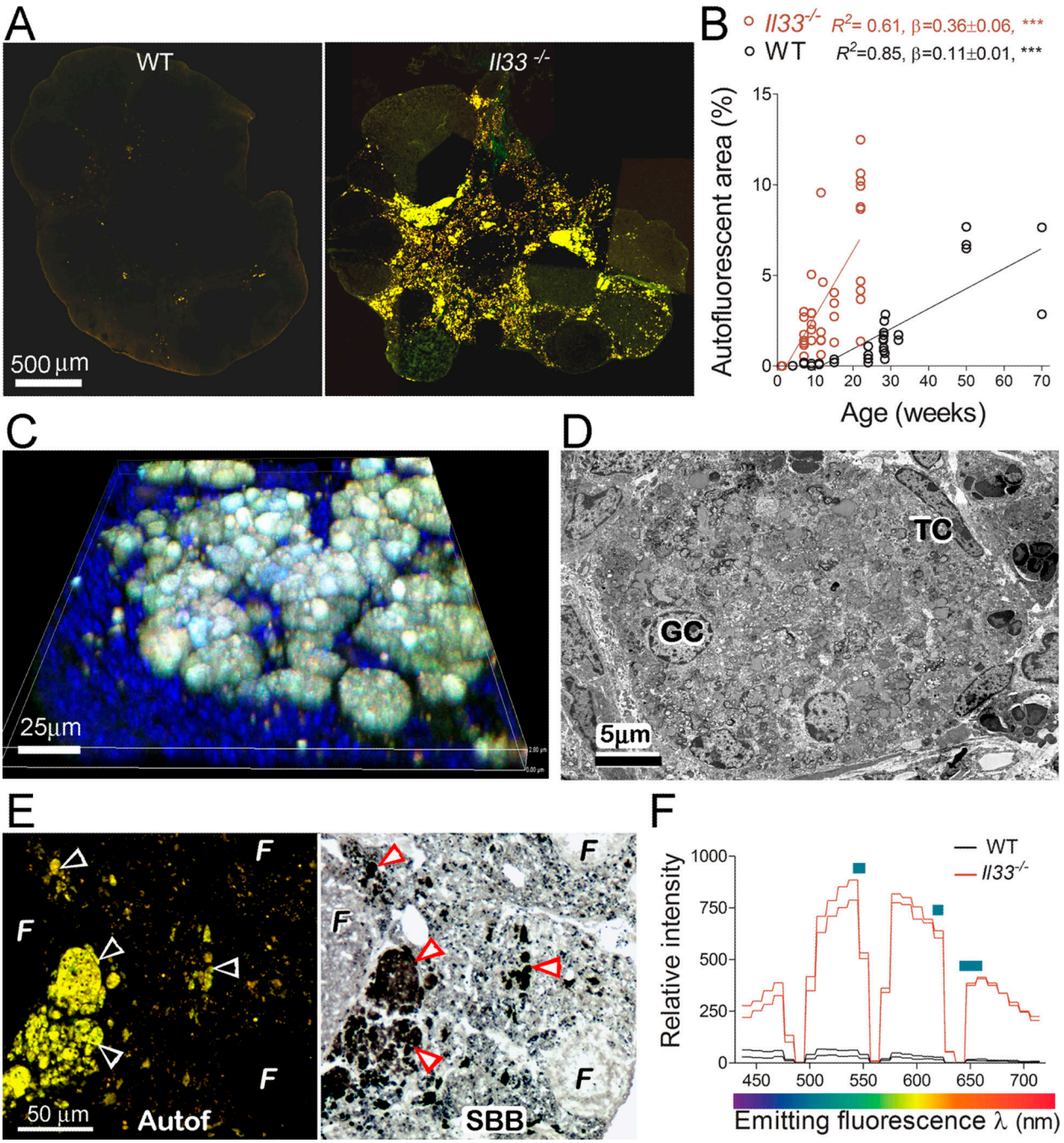

FIGURE 2.

Deletion of the *Il33* gene in mice leads to a massive accumulation of abnormally degrading atretic follicles in the ovaries. (**A**) Fluorescent micrographs show the presence of large quantities of autofluorescent materials in a 15 weeks $Il33^{-/-}$ mouse (right panel) but not in an age-matched WT mouse (left panel). (**B**) Time course for accumulation of autofluorescent materials in the ovaries of WT and $Il33^{-/-}$ mice. Autofluorescence is quantified as area % of entire ovarian section. (**C**) 3D confocal fluorescent micrograph shows numerous spherical bodies emitting autofluorescence. Nuclei were counterstained by

DAPI. (**D**) Ultrastructure of an autofluorescent body by electron microscopy. It contains multiple intact granulosa cell nuclei (GC) and theca cells (TC) mixed with numerous collapsing organelles. Also notice an absence of any intact cell membranes. (**E**) Detection of abundant lipofuscin in autofluorescent bodies on ovarian section of *Il33*$^{-/-}$ mice. Paired arrowheads indicate a complete overlap of autofluorescence (left panel) with Sudan Black B staining for lipofuscins (right panel). Note the absence of autofluorescence in normal follicles (*F*). (**F**) Fluorescent spectra of atretic follicles in *Il33*$^{-/-}$ or WT ovaries. Two representative samples (total 5) for each group are shown. Blue bars indicate emitting peak ranges for lipofuscins.

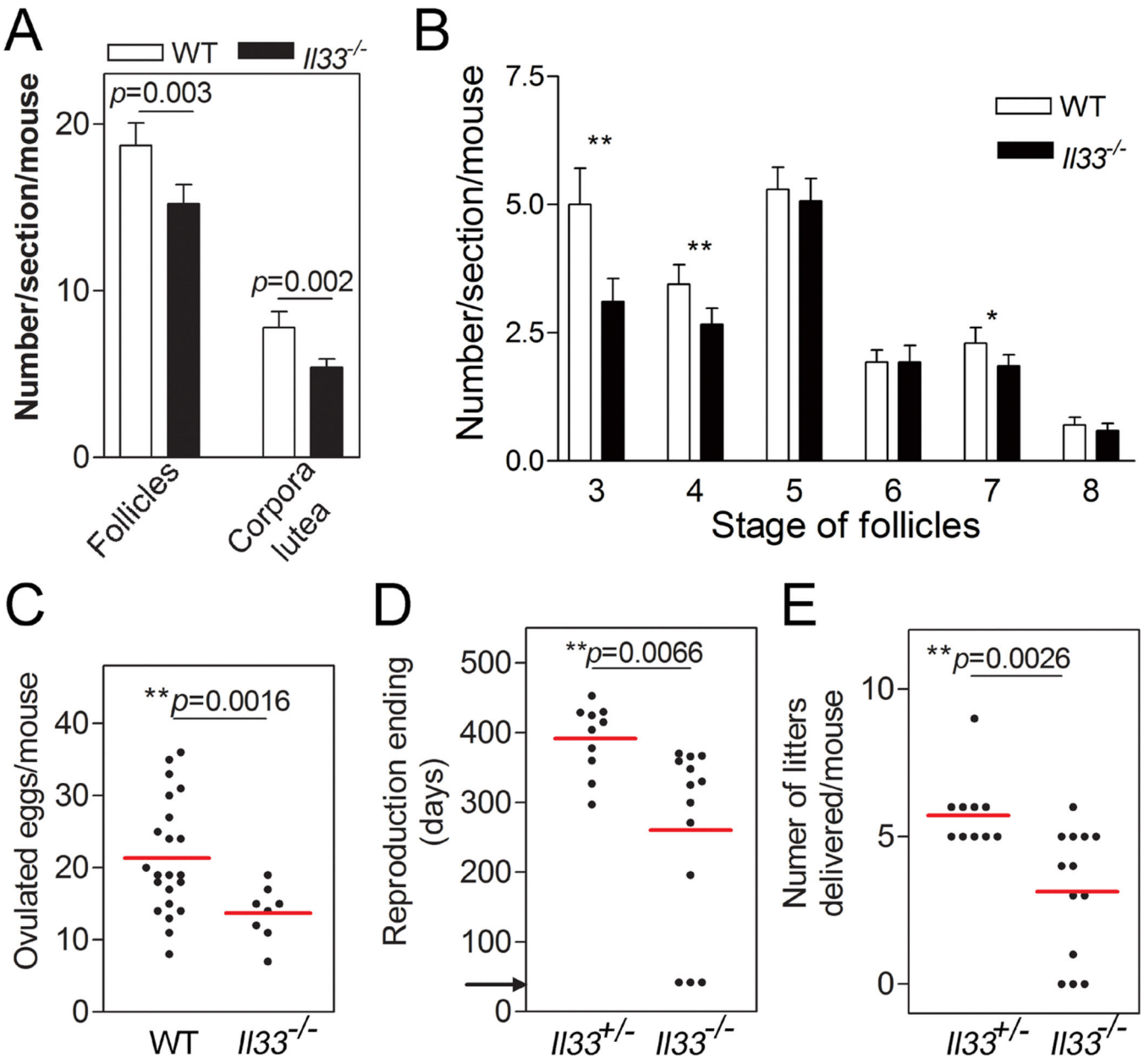

FIGURE 3.

Accelerated ovarian aging and shortened reproductive lifespan in *Il33*$^{-/-}$ female mice. (**A**) Statistical analyses of normal and atretic follicles in 15–20 week-old mice on H-E stained ovarian sections. Normal follicles include those with more than one layer of granulosa cells to those with an antrum. From serial sections through an entire ovary, three with the largest areas were chosen for counting. (**B**) Statistics of different types of developing follicles (14). Six mice from each group were sampled and analyzed by two-tailed *t*-test. Error bars represent the S.E.M. (**C**) Ovulated eggs after hCG-induced ovulation in 15–20 week old *Il33*$^{-/-}$ or WT mice. Eggs were collected at 13 hours post hCG injection and counted. Two-tailed *t*-test was applied. Data pooled from two independent experiments. Total 4 experiments were performed with similar results. (**D**) Reproductive lifespan in *Il33*$^{-/-}$

females and their *Il33*$^{+/-}$ littermates under continuous mating with fertile males. Ages for their last successful delivery of a litter were recorded as the end of their reproductive life. Mice were randomly selected from five litters of different parents. Arrow indicates the starting mating age (6 weeks). (**E**) Number of litters successfully delivered by each mouse during their entire reproductive life. The data were based on the same mice as those used in D. Two-tailed *t*-test was applied. Red bars represent mean of a group.

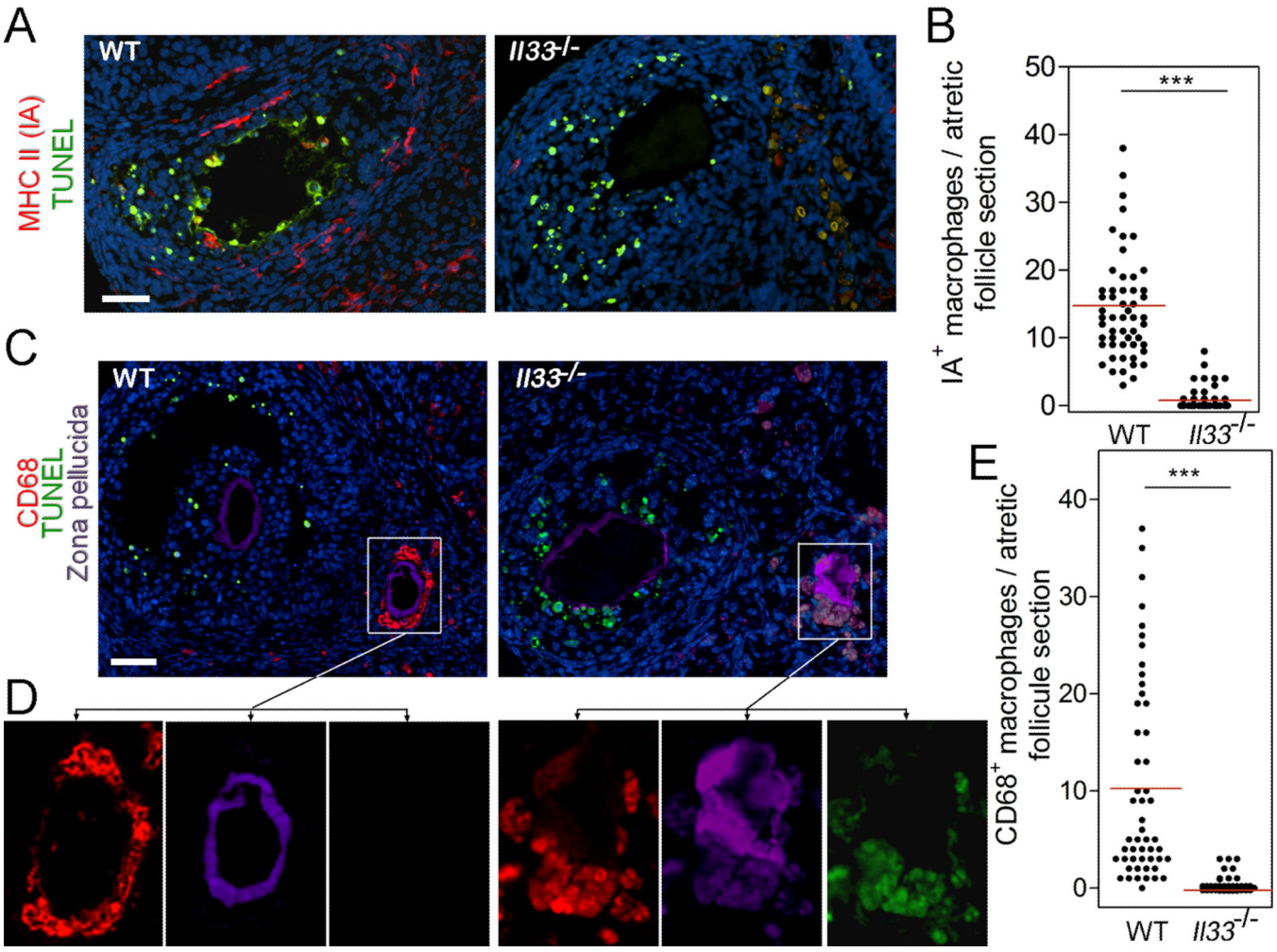

FIGURE 4.

Impaired migration of macrophages into atretic follicles in *Il33*$^{-/-}$ mice. (**A**) Detection of invasion of MHC class II-expressing IA^{+} macrophages (red) into atretic follicles by immunofluorescence. Early stage of atresia is indicted by the presence of apoptotic follicular cells as revealed by TUNEL staining (green). IA^{+} macrophages (red) are present in the early atretic follicle in WT mice (left panel), but absent in *Il33*$^{-/-}$ mice (right panel). (**B**) Statistical distribution of IA^{+} macrophages in each atretic follicle in WT or *Il33*$^{-/-}$ mice. Red bars represent mean of a group. (**C**) Detection of migration of CD68^{+} macrophages (red) into follicles. Left panel shows cluster of CD68^{+} macrophages around collapsing zone pellucida (purple) of an follicle at mid atresia in a WT mouse; CD68^{+} macrophages are absent in a follicle at early stage of atresia with apoptotic cells (green). Right panel shows absence of CD68^{+} macrophages in any follicles in an *Il33*$^{-/-}$ mouse. Bar = 50 μm. (**D**) Two sets of panels show separated three fluorescent channels for each squared area in C, respectively, as connected by arrows. Autofluorescent materials around zone pellucida in follicle at mid atresia of *Il33*$^{-/-}$ mice are demonstrated by a complete overlap of fluorescence from three channels (right set of panels). (**E**) Statistical distribution of CD68^{+}

macrophages in each atretic follicle at mid atresia in WT and *Il33*$^{-/-}$ mice. Red bars represent mean of a group. Bars in A, C = 50 μm.

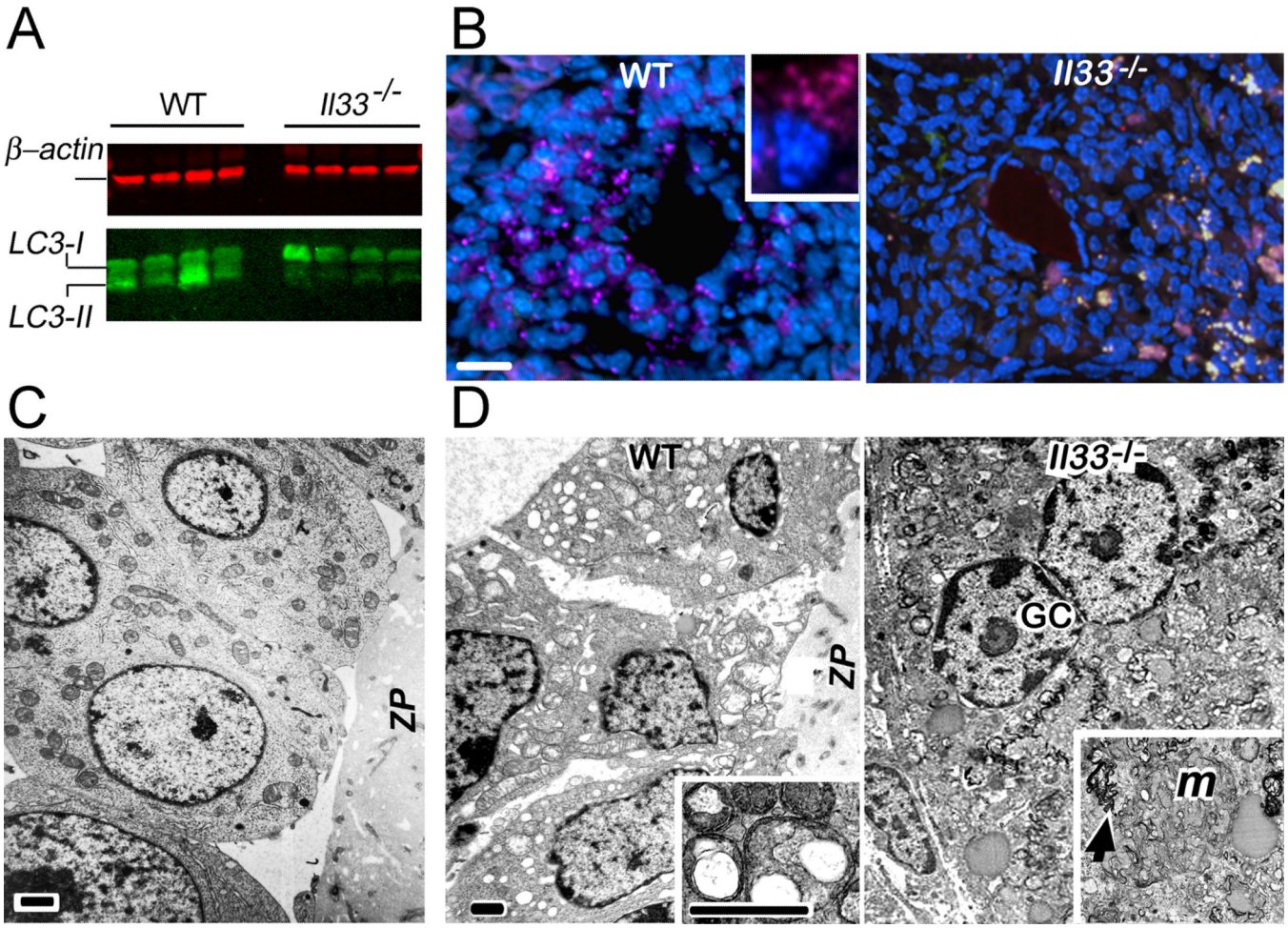

FIGURE 5.

Diminished autophagy in atretic follicles in *Il33*$^{-/-}$ mice. (**A**) Western blot detection of ovarian LC3 in four representative WT or *Il33*$^{-/-}$ mice. Notice lower quantities of LC3-II in *Il33*$^{-/-}$ ovaries than those for WT mice. Both mice show a comparable level of LC3-I. β–actin (red) is simultaneously detected in the same blots and used as a protein quantity control. This experiment was repeated three times with similar results. (**B**) Detection of autophagosomes as LC3^{+} subcellular granules (purple) in follicles at mid atresia by immunofluorescence. LC3^{+} granules are present in follicular cells in WT mice (left panel). Inset shows an enlarged follicular cell with LC3^{+} granules. Right panel shows absence of LC3^{+} in an atretic follicle of an *Il33*$^{-/-}$ mouse with many irregular autofluorescent granules (whitish). Notice that deformation of follicles due to atresia is similar in *Il33*$^{-/-}$ and WT mice. Bar = 50 μm. (**C**) Ultrastructure of granulosa cells near zona pellucida (ZP) of a normal follicle shown by electron microscopy. (**D**) Ultrastructures of granulosa cells in atretic follicles. A group of granulosa cells surrounding zona pellucida of an atretic follicle in WT mice show numerous autophagous vacuoles in their cytoplasm with relative intact nuclei (left panel). Inset shows double-membraned autophagosomes with degrading organelles. Right panel shows a collapsing atretic follicle in *Il33*$^{-/-}$ mice without any vacuoles in granulosa cells. Relatively intact granulosa cell nuclei (*GC*) are present. No cell

membranes and cell boundaries are seen. Degrading organelles such as swollen mitochondria (*M*) and fragmented cytoplasm membranes (arrow) are dislocated and mixed (inset). Bars in C, D = 2 μm.